JOURNAL OF GEOPHYSICAL RESEARCH, VOL. 106, NO. C8, PAGES 16,841–16,855, AUGUST 15, 2001

# A numerical study of wave-current interaction through surface and bottom stresses: Wind-driven circulation in the South Atlantic Bight under uniform winds

Lian Xie , Kejian Wu,[1] Leonard Pietrafesa, and Chen Zhang

Department of Marine, Earth, and Atmospheric Sciences, North Carolina State University, Raleigh, North Carolina

**Abstract.** The influences of surface waves on ocean currents in the coastal waters of the South Atlantic Bight are investigated by using a coupled wave-current modeling system. The ocean circulation model employed is the three-dimensional Princeton Ocean Model (POM), and the wave model invoked is an improved third-generation wave model (WAM). The coupling procedure between the POM and the WAM and the simulated coastal ocean circulation driven by uniform surface winds are presented. The simulated results show that wind waves can significantly affect coastal ocean currents not only through an enhancement of wind stress but also through a modification of bottom stress. Wave-induced wind stress increases the magnitude of currents both at the surface and near the seabed. On the other hand, wave-induced bottom stress weakens the currents both at the sea surface and near the seabed. Therefore the net effect of surface wind waves on currents depends on the relative importance of current modulations by wave-induced wind stress and bottom stress. The results further indicate that at a fixed location, the relative importance of wave-induced surface and bottom shear stresses in coastal ocean circulation depends on the surface wind field. For the constant wind cases considered in this study, the effect of wave-induced bottom stress is more significant in along-shore wind conditions than in cross-shore wind conditions.

## 1. Introduction

When winds blow over water, currents and surface waves are generated contemporaneously. Wind-induced currents, surface waves, and interactions between them are critical factors for many physical processes in the ocean such as the transport of mass, momentum, and energy, coastal upwelling, storm surge, and air-sea interactions. These physical processes further affect chemical and biological processes such as the dispersion of pollutants and transport of biota. Existing wave-current interaction models [*Tolman*, 1990; *Holthuijsen and Tolman*, 1991; *Masson*, 1996] have focused mainly on the influence of currents on waves. However, in many circumstances, surface waves also play an important role in determining the ocean current fields. For example, large surface waves typically accompany storm surge under the influence of tropical and extratropical cyclones. These wind waves can not only cause direct damage to coastal structures but also contribute to the overall storm surge [*Mastenbroek et al.*, 1993; *Komen et al.*, 1994].

Generally speaking, surface waves affect ocean currents in the following ways: (1) increasing the surface roughness length and thus enhancing the effective wind stress [*Donelan et al.*, 1993], (2) increasing the bottom stress in shallow waters where the wave's orbital velocity below the sea surface is large enough to influence the bottom currents [*Christofferson and Jonsson*, 1985], and (3) interacting with the current field through radiation stress [*Longuet-Higgins and Stewart*, 1962]. Surface waves may also affect currents in other ways, such as through the wave-induced Stokes' drift and the Coriolis wave stress [*Huang*, 1977; *Jenkins*, 1987]. How to incorporate these effects into an ocean circulation model has been the subject of several recent studies. For example, *Davies and Lawrence* [1995] examined the effect of surface waves on the bed friction factor and on the currents in a three-dimensional current model. They showed that for waves with periods longer than 10 s, the bottom friction is significantly enhanced and causes a reduction in near-bed currents. *Davies and Lawrence* [1995] used a prescribed surface wave field with constant amplitude and wave period and thus did not consider the effect of currents on waves and the effect of waves on wind stress. On the other hand, *Donelan et al.* [1993] investigated the effect of surface waves on wind stress and proposed an empirical model for the estimation of surface roughness length in the presence of surface waves. In this case, the total surface shear stress can be computed as the sum of the wave-independent wind stress and the wave-induced shear stress. *Komen et al.* [1994] documented that by including the wave-induced surface shear stress, the maximum height of the storm surge predicted by a wave-current coupled model can be significantly improved.

[1] Now at Inst. Of Physical Oceanography, Ocean Univ. of Quingdao, Quingdao, China



Paper number 2000JC000292
0148-0227/01/2000JC000292$09.00

The purpose of this study is to better understand the physical mechanisms of wave-current interaction in the presence of both wave-induced surface and bottom shear stresses using a coupled wave-current modeling system. This study extends that of *Davies and Lawrence* [1995] by including an explicit simulation of the wave field and the coupling of waves and currents through both surface and bottom shear stresses. Brief descriptions of the coastal ocean circulation model and the wave model are given in section 2. The coupling procedure is described in section 3. Section 4 introduces the geographical settings of the study area and the designs of the modeling experiments. The simulated effects of wind waves on surface and near-bed ocean currents under a constant wind are discussed in section 5, followed by a discussion of the sensitivity of the model results to wind directions in section 6. Main conclusions are summarized in section 7.

## 2. Model Descriptions

The coupled wave-current modeling system is based on the well-known Princeton Ocean Model (POM) [*Mellor*, 1996] and the third-generation wave model (WAM Cycle 4) [*Komen et al.*, 1994]. A brief description of the POM and the WAM, and modifications to the two models as well as the coupling procedure, is presented below.

### 2.1. Circulation Model

The POM is a three-dimensional, primitive-equation model that uses a sigma $[\sigma=(z-\eta)/D]$ coordinate in the vertical, a curvilinear orthogonal coordinate ($x$ and $y$) and an "Arakawa C" grid scheme in the horizontal. Here $D$ is the total water depth, $z$ is the distance from the mean sea surface, and $\eta$ is the water level departure from the unperturbed sea surface. The POM contains an embedded second moment turbulence closure submodel to provide vertical mixing coefficients. The model has a free surface elevation and a split-step time step. It has been used to describe the evolution of the oceanic mixed layer [*Large and Crawford*, 1995] and the response of the Gulf Stream to cold air out breaks [*Xue and Bane*, 1997]. More recently, *Xie et al.* [1998, 1999a,b] used this model to study the response of the Carolina coastal ocean to Hurricane Fran and found that significant differences exist between the responses of the coastal ocean versus those of deep waters to a moving hurricane.

The nonlinear momentum equations used in the POM model can be written as

$$\frac{\partial UD}{\partial t}+\frac{\partial U^2D}{\partial x}+\frac{\partial UVD}{\partial y}+\frac{\partial U\Omega}{\partial \sigma}-fVD+gD\frac{\partial \eta}{\partial x}+\frac{gD^2}{\rho_0}\int_\sigma^0\left[\frac{\partial \rho'}{\partial x}-\frac{\sigma'}{D}\frac{\partial D}{\partial x}\frac{\partial \rho'}{\partial \sigma'}\right]d\sigma'=\frac{\partial}{\partial \sigma}\left[\frac{K_M}{D}\frac{\partial U}{\partial \sigma}\right]+F_x \quad (1)$$

$$\frac{\partial VD}{\partial t}+\frac{\partial UVD}{\partial x}+\frac{\partial V^2D}{\partial y}+\frac{\partial V\Omega}{\partial \sigma}+fUD+gD\frac{\partial \eta}{\partial y}+\frac{gD^2}{\rho_0}\int_\sigma^0\left[\frac{\partial \rho'}{\partial y}-\frac{\sigma'}{D}\frac{\partial D}{\partial y}\frac{\partial \rho'}{\partial \sigma'}\right]d\sigma'=\frac{\partial}{\partial \sigma}\left[\frac{K_M}{D}\frac{\partial V}{\partial \sigma}\right]+F_y \quad (2)$$

and the mass conservation equation as

$$\frac{\partial DU}{\partial x}+\frac{\partial DV}{\partial y}+\frac{\partial \Omega}{\partial \sigma}+\frac{\partial \eta}{\partial t}=0 \quad (3)$$

Here $U$ and $V$ are the two horizontal velocity components in the $x$ and $y$ directions, respectively, $\Omega$ is the velocity component normal to $\sigma$ surfaces, $D=h+\eta$ , $h(x,y)$ is the unperturbed water depth defined by the bottom topography, and $\eta(x,y,t)$ is the surface elevation above the mean sea level. The value of $\sigma$ ranges from $\sigma=0$ at $z=\eta$ to $\sigma=-1$ at $z=-h$; $F_x$ and $F_y$ are horizontal momentum diffusion terms parameterized according to *Smagorinsky* [1963]. They are related to the subgrid-scale mixing processes, which are not directly resolved by the model. $g$ is the gravitational acceleration, $t$ is time, $f$ is the Coriolis parameter, $\rho_0$ is the reference density, and $\rho$ is the density at sigma level $\sigma$. The first term on the right-hand sides of (1) and (2) are parameterized Reynolds stresses, where $K_M$ is the turbulent diffusion coefficient of momentum modeled according to the second-order turbulence closure scheme of *Mellor and Yamada* [1982]. The original POM model also contains prediction equations of temperature and salinity which, in the present application, are prescribed.

The atmospheric wind forcing is applied at the sea surface through the following surface wind stress

$$\tau_a=\rho C_D|\boldsymbol{U}_{10}|\boldsymbol{U}_{10} \quad (4)$$

where $\rho_a$ is the air density, $C_D$ is the drag coefficient at the air-sea interface, and $\boldsymbol{U}_{10}$ is the surface (10 m above mean sea level) wind speed. The bottom stress is similarly estimated by

$$\tau_b=\rho C_b|\boldsymbol{U}_C|\boldsymbol{U}_C \quad (5)$$

where $C_b$ is the drag coefficient in the ocean bottom boundary layer, and $\boldsymbol{U}_C$ is the bottom current vector, and $\rho$ is water density. In wave-current coupled simulations, $C_b$ is determined by a sea state-dependent friction parameter (see section 3 for details).

Equations (1)-(5) are used in the POM. In order to couple the circulation model to the wave model, these equations must be modified to include the effect of waves.

First, the radiation stresses due to direct wave-current interactions need to be added to the right-hand side of (1) and (2). It is well known [e.g., *Longuet-Higgins and Stewart*, 1962] that for a unit mass of water the radiation stress forcing in the $x$ and $y$ directions can be written, respectively, as

$$T_x=-\frac{1}{\rho(h+\eta)}\left(\frac{\partial S_{xx}}{\partial x}+\frac{\partial S_{xy}}{\partial y}\right) \quad (6)$$

$$T_y=-\frac{1}{\rho(h+\eta)}\left(\frac{\partial S_{yx}}{\partial x}+\frac{\partial S_{yy}}{\partial y}\right) \quad (7)$$

where the radiation stress tensor is

$$S=\begin{pmatrix}S_{xx} & S_{xy}\\ S_{yx} & S_{yy}\end{pmatrix} \quad (8)$$

with $S_{xy}=S_{yx}$. Following *Lewis* [1998], (1) and (2) can then be rewritten as

$$\frac{\partial UD}{\partial t}+\frac{\partial U^2D}{\partial x}+\frac{\partial UVD}{\partial y}+\frac{\partial U\Omega}{\partial \sigma}-fVD+gD\frac{\partial \eta}{\partial x}$$

$$+\frac{gD^2}{\rho_0}\int_\sigma^0\left[\frac{\partial\rho'}{\partial x}-\frac{\sigma'}{D}\frac{\partial D}{\partial x}\frac{\partial\rho'}{\partial\sigma'}\right]d\sigma'$$

$$=\frac{\partial}{\partial\sigma}\left[\frac{K_M}{D}\frac{\partial U}{\partial\sigma}\right]+F_x+T_x \tag{9}$$

$$\frac{\partial VD}{\partial t}+\frac{\partial UVD}{\partial x}+\frac{\partial V^2D}{\partial y}+\frac{\partial V\Omega}{\partial\sigma}+fUD+gD\frac{\partial\eta}{\partial y}$$

$$+\frac{gD^2}{\rho_0}\int_\sigma^0\left[\frac{\partial\rho'}{\partial y}-\frac{\sigma'}{D}\frac{\partial D}{\partial y}\frac{\partial\rho'}{\partial\sigma'}\right]d\sigma'$$

$$=\frac{\partial}{\partial\sigma}\left[\frac{K_M}{D}\frac{\partial V}{\partial\sigma}\right]+F_y+T_y \tag{10}$$

For convenience, hereinafter we will refer to the modified POM, which utilizes (9) and (10), as the NCPOM.

### 2.2. Wave Model

The wave model used in this study is based on the third-generation wave model, WAM Cycle 4 [*Komen et al.*, 1994]. The model is constructed by solving the following ocean wave spectral transport equation

$$\frac{\partial F}{\partial t}+\nabla\cdot\left(\left(\vec{C}_g+\vec{V}\right)F\right)+\frac{\partial}{\partial\theta}\left(C_\theta F\right)+\frac{\partial}{\partial\omega}\left(C_\omega F\right)=G \tag{11}$$

where $F(\omega,\theta;x,y,t)$ is the ocean wave directional spectrum, $\omega$ is the frequency, $\theta$ is the direction of wave component, $\vec{C}_g$ is wave group velocity, $\vec{V}$ is the mean current, $C_\theta$ and $C_\omega$ are the transport velocity of directional spectrum in $\theta$ and $\omega$ space, respectively, and $G$ is the sum of the source function, being

$$G=S_{in}+S_{nl}+S_{dis} \tag{12}$$

where $S_{in}$, $S_{nl}$, and $S_{dis}$ represent, respectively, the physics of wind input, nonlinear wave-wave interaction and wave energy dissipation due to wave breaking and bottom friction. The third term on the left-hand side of (11) describes the refraction due to current effects, and the fourth term describes the energy redistribution due to frequency transformation.

In the WAM model the wind input term is given by

$$S_{in}=\gamma\cdot F, \tag{13}$$

where $\gamma$, the growth rate of the waves, is related to wind forcing. It is modeled according to *Snyder et al.* [1981] and is consistent with the theory of *Miles* [1957].

The nonlinear wave-wave interaction term represents the nonlinear, conservative energy exchanges between all possible quadruplet wave components satisfying the following resonance conditions for wave number $\boldsymbol{k}$ and frequency $\omega$

$$\boldsymbol{k}_1+\boldsymbol{k}_2-\boldsymbol{k}_3=\boldsymbol{k}_4 \tag{14}$$

$$\omega_1+\omega_2-\omega_3=\omega_4 \tag{15}$$

where components 1, 2, and 3 exchange energy with component 4. The equations and discrete interaction approximation method needed to compute the nonlinear wave-wave interaction are given by *Hasselmann and Hasselmann* [1985] and *Hasselmann et al.* [1985].

The dissipation term relates to two mechanisms of wave energy dissipation with respect to water depth. In deep water, energy dissipation due to wave breaking is dominant. This process can be described mathematically as

$$S_{br}=\gamma_d\cdot F, \tag{16}$$

where $\gamma_d$ is the dissipation rate due to wave breaking based on *Komen et al.* [1984]. In shallow waters, energy dissipation can be caused by several physical processes, which are dependent on the conditions of the ocean floor. However, in the WAM, only bottom friction is considered in the shallow waters outside the surf zone. The bottom friction term is given as a linear expression obtained from the Joint North Sea Wave Project Experiment [*Hasselmann et al.*, 1973]:

$$S_{bf}=-\frac{\Gamma}{g^2}\frac{\omega^2}{\sinh^2(kh)}F \tag{17}$$

where $\Gamma$ is a constant, $k$ is the magnitude of the wave number, and $g$ is gravity. In the surf zone, both wave breaking and bottom friction processes are considered.

Generally speaking, when ocean waves propagate through a spatially and temporally varying current, their properties can be significantly affected due to wave-current interactions. The influences of currents on surface waves induced by wave-current interactions can not only kinematically change the wave frequency and wave number but also dynamically affect wave fields via the radiation stress. Equation (11) describes the wave evolution in a slowly varying current ($\vec{V}$), and it only considers wave-current interactions kinematically. In order to consider wave-current interactions both kinematically and dynamically, it is necessary to incorporate the radiation stress ($\vec{T}:\nabla\vec{V}$) into the spectral transport equation. This can be achieved either by converting (11) into wave action balance equation [*Lin* and *Huang*, 1996a,b] or by adding the radiation stress term directly to (11). The latter approach involves explicit computation of radiation stress, which is needed in the circulation model as a coupling mechanism. After doing so, (11) becomes [*Phillips*, 1977]

$$\frac{\partial F}{\partial t}+\nabla\cdot\left(\left(\vec{C}_g+\vec{V}\right)F\right)+\frac{\partial}{\partial\theta}\left(C_\theta F\right)+\frac{\partial}{\partial\omega}\left(C_\omega F\right)+\vec{T}:\nabla\vec{V}=G. \tag{18}$$

Here the radiation stress tensor $\vec{T}$ is expressed as

$$\vec{T}=\frac{F}{2}\begin{pmatrix}2n(1+\cos^2\theta)-1 & n\sin 2\theta\\ n\sin 2\theta & 2n(1+\sin^2\theta)-1\end{pmatrix}, \tag{19}$$

where

$$n=\frac{1}{2}+\frac{kh}{\sinh(2kh)}. \tag{20}$$

Equation (18) is the governing equation for surface wind waves used in the present study. For convenience, we will refer to the modified WAM as the NCWAM.

## 3. Coupling between Waves and Currents

### 3.1. Coupling through Surface Shear Stress

It has long been recognized that surface wind stress over water is directly correlated with the surface wind vector multiplied by its absolute value. However, considerable uncertainty remains in the exact relationship between wind stress and wind via the drag coefficient, particularly in the presence of wave-induced surface roughness. In the last decade, significant progress has been made

on the effects of surface waves on wind stress [*Smith et al.*, 1992; *Donelan et al.*, 1993, and references therein]. Intuitively, when wind blows over the sea surface, surface waves are generated, and these surface waves can, in turn, modify the surface roughness. Thus when estimating the drag coefficient, both wind speed and surface wave effects should be taken into account.

In this study the effect of surface waves on the drag coefficient will be incorporated into the circulation model through the use of the empirical model of *Donelan et al.* [1993] which computes the roughness length according to

$$z_0 = 3.7\times10^{-5}\frac{U_{10}^2}{g}\left(\frac{U_{10}}{C_p}\right)^{0.9} \tag{21}$$

where $C_p$ is the wave speed corresponding to the spectral peak frequency, $U_{10}$ is the wind speed at 10 m above the mean sea level, and $U_{10}/C_p$ represents the wave age. Since wave age characterizes the wave development stages, the wind stress is determined by both the 10 m wind and wave states.

### 3.2. Wave-Current Coupling through Bottom Stress

Surface waves can not only affect the currents by modifying the drag coefficient but also affect the current field in shallow water regions by modifying the bed stress. The orbital velocity of wind waves decreases rapidly with depth below the sea surface. But in shallow waters when the effect of wind waves is strong enough to reach the bottom boundary layer, turbulent mixing can be enhanced by the wave effects and, consequently, bottom stress can be modified by wave-current interactions [*Grant and Madsen*, 1979].

*Davies and Lawrence* [1995] examined the effects of the wave-induced bottom stress on the currents in shallow waters by using a three-dimensional, wind-driven circulation model with prescribed surface wind waves of constant amplitudes and periods. They considered the mechanism proposed by *Grant and Madsen* [1979] and the computational approach suggested by *Signell et al.* [1990]. The study by *Davies and Lawrence* [1995] indicated that surface waves can significantly affect the currents by modifying the bed friction coefficient in shallow waters.

In the present study the same procedure proposed by *Signell et al.* [1990] and used by *Davies and Lawrence* [1995] will be adopted to compute the wave-enhanced friction coefficient $f_c$. A brief description of this procedure is presented below.

For simplicity, only the procedure applicable to collinear waves and currents are described, though extension to waves and currents at an arbitrary angle is not complicated. Detailed discussion of this procedure and other relevant references are given by *Signell et al.* [1990].

At the seabed, in the absence of wind waves, the bottom stress components $F_B$ and $G_B$ can be related to the near-bed currents $U_c$ and $V_c$ using a quadratic friction law

$$F_B=0.5f_c\rho U_c(U_c^2+V_c^2)^{1/2} \tag{22}$$

$$G_B=0.5f_c\rho V_c(U_c^2+V_c^2)^{1/2} \tag{22}$$

The total bed shear stress $\tau_b$ can be decomposed into the maximum wave bed stress $\tau_w$ and instant current bed stress $\tau_c$, namely,

$$\tau_b=\tau_c+\tau_w \tag{24}$$

$$\tau_w=0.5f_w\rho U_w^2 \tag{25}$$

where $U_w$ is the maximum near-bed wave orbital velocity depending on water depth and $f_w$ is the wave friction factor.

The near-bed wave orbital velocity is given by

$$U_w=a_w\omega/\sinh kh, \tag{26}$$

where $a_w$ is the wave amplitude, $\omega$ is the wave frequency, and $k$ is the wave number determined from the linear dispersion relation

$$\omega^2=(gk)\tanh(kh). \tag{27}$$

The values of $f_w$ can be computed from the semiempirical expression of *Jonsson* [1967] and *Jonsson and Carlsen* [1976] which was derived based upon laboratory observations:

$$\frac{1}{4\sqrt{f_w}}+\log_{10}\left(\frac{1}{4\sqrt{f_w}}\right)=-0.08+\log_{10}\left(\frac{A_b}{k_b}\right). \tag{28}$$

For the calculation of the current friction factor $f_c$, taking the wind waves into account, we follow *Davies and Lawrence* [1995] and *Signell et al.* [1990], using

$$f_c=2\left[\frac{K}{\ln(30z_r/k_{bc})}\right], \tag{29}$$

with $z_r$ being the reference height at which the slip condition is applied, taken here as 100 cm. Initially, $k_{bc}$ is taken as the Nikuradse roughness $K_b=30z_0$ and $z_0=0.146\times10^{-2}$ m.

Having determined the initial values of the wave friction factor $f_w$ and current friction factor $f_c$, we can readily use the following iterative method to compute the effective drag coefficient $f_c$, taking into account the surface wave effects. The wave friction velocity $U_{*w}$ and current friction velocity $U_{*c}$ can then be computed from

$$U_{*w}=\left(\frac{\tau_w}{\rho}\right)^{1/2}, \tag{30}$$

$$U_{*c}=\left(\frac{\tau_c}{\rho}\right)^{1/2}. \tag{31}$$

Next the combined friction velocity $U_{*\mathrm{CW}}$ for currents and waves is given by

$$U_{*cw}=(U_{*c}^2+U_{*w}^2)^{1/2}. \tag{32}$$

The apparent bottom roughness $k_{bc}$ due to wave-current interaction can then be computed from

$$k_{bc}=k_b\left[24\frac{U_{*cw}}{U_w}\frac{A_b}{k_b}\right]^{\beta} \quad \text{with} \quad \beta=\left(1-\frac{U_{*c}}{U_{*cw}}\right), \tag{33}$$

where $A_b=U_w/\omega$ is the near-bottom excursion amplitude.

The new value of $k_{bc}$ computed from (33) is used in (29) to obtain an updated value of $f_c$. Through this iterative process we can compute the final value of $f_c$ which includes the effects of wave-current interaction. This final value of $f_c$ will then be used to compute the bed stress components $F_B$ from (22) and $G_B$ from (23) in the three-dimensional circulation model.

### 3.3. Wave-Current Interaction through Radiation Stress

In the present study we will directly calculate the radiation stress from the wave momentum flux formula [*Longuet-Higgins and Stewart*, 1962]

$$S_{ij}=E\left[\frac{k_ik_j}{k^2}\frac{C_g}{C}+\left(\frac{C_g}{C}-\frac{1}{2}\right)\delta_{ij}\right], \tag{34}$$

where $E$ is the wave kinematic energy density, $k$ is the wave number, $k_i$ and $k_j$ are the two components of the wave number

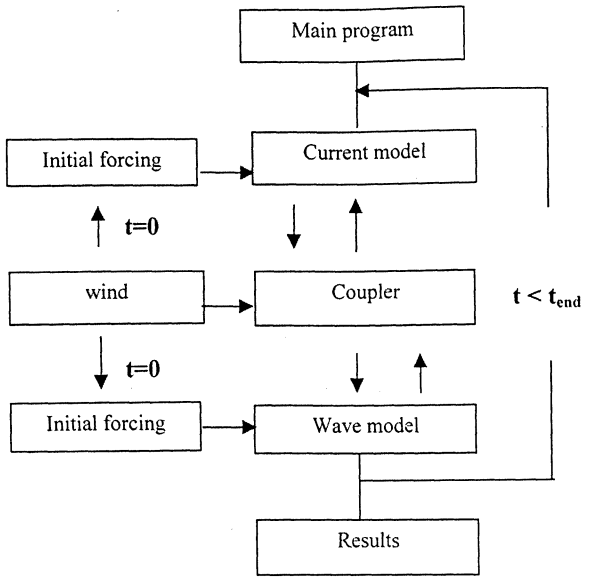


**Figure 1.** Flow diagram illustrating the coupling process between the wave and the current model.

vector, respectively, $C$ is the wave speed, $C_g$ is the group speed, and $\delta_{ij}$ is the Kronecker $\delta$ tensor. We have

$$\frac{C_g}{C} = n, \qquad n = \frac{1}{2} + \frac{kd}{sh(2kd)}, \tag{35}$$

with $a$ being the wave amplitude. Assuming that the angle between the wave direction and the $x$ axis is $\varphi$ and the wave number components are $k_i=k_1=\cos\varphi$, and $k_j=k_2=\sin\varphi$, then the radiation stress can be expressed as

$$S_{xx} = S_{11} = E\left[\frac{C_g}{C}\cos^2\varphi + \left(\frac{C_g}{C} - \frac{1}{2}\right)\right], \tag{36}$$

$$S_{yy} = S_{22} = E\left[\frac{C_g}{C}\sin^2\varphi + \left(\frac{C_g}{C} - \frac{1}{2}\right)\right], \tag{37}$$

where

$$S_{xy} = S_{yx} = S_{12} = S_{21} = E\frac{C_g}{C}\sin\varphi\cos\varphi. \tag{38}$$

All above results are obtained from monochronic wave theory. Assuming that the above equations are suitable for the component waves in the wave directional spectrum described by linear random wave theory, the radiation stress for realistic ocean waves can then be written as

$$S_{ij} = \rho g \int_{-\pi}^{\pi}\int_{\omega_1}^{\omega_2}\left[\frac{k_i k_j}{k^2}\frac{C_g}{C} + \left(\frac{C_g}{C} - \frac{1}{2}\right)\delta_{ij}\right]F(\omega,\theta)\,d\theta\,d\omega, \tag{39}$$

where $F(\omega,\theta)$ is the frequency directional spectrum, and $\omega_1$ and $\omega_2$ are the lower and upper limits of frequency in the numerical wave model, respectively. All of the wave parameters, including the directional spectrum, can be calculated from the wave model. The effects of radiation stress on currents can then be computed by the substitution of the radiation stress into the right-hand sides of (9), (10), via (39).

### 3.4. Coupling Procedure

After incorporating the above three types of wave effects into the circulation model (NCPOM), the coupling of the wave model and the circulation model is straightforward. This is illustrated in Figure 1. It describes the coupling process between the wave model (NCWAM) and current model (NCPOM). The idea is to exchange the simulated data between the wave model and the current model at every time step. In other words, the current field

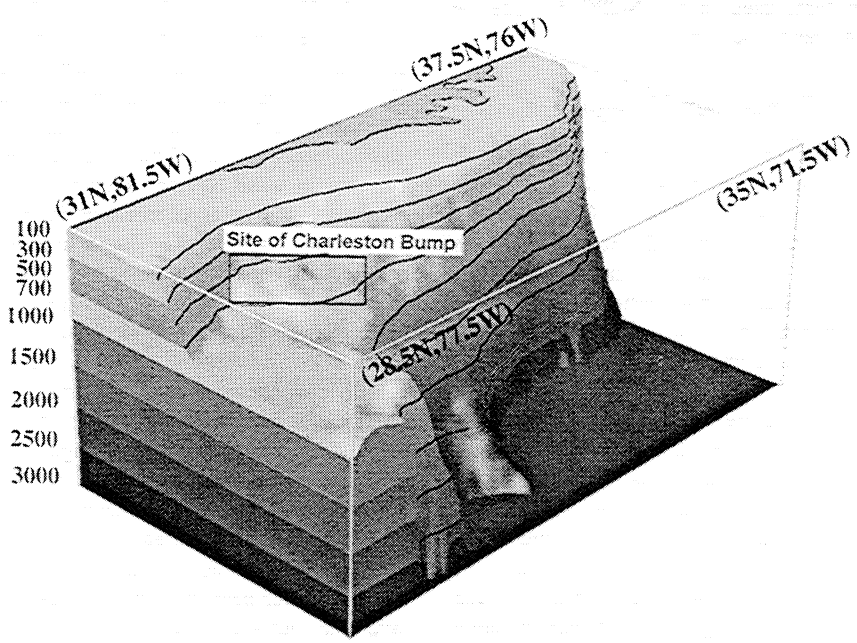


**Figure 2.** A three-dimensional depiction of the study area and bathymetry.

**Table 1.** List of Experiments

| Experiment | Cases | Wind Direction (deg) | Wave-Induced Surface Stress | Wave-Induced Bottom Stress |
|---|---|---|---|---|
| 1 | NN | 0 (360) | no | no |
| 2 | YN | 0 (360) | yes | no |
| 3 | NY | 0 (360) | no | yes |
| 4 | YY | 0 (360) | yes | yes |
| 5 | $S_{NN1}$ | 45 | no | no |
| 6 | $S_{NN2}$ | 90 | no | no |
| 7 | $S_{NN3}$ | 135 | no | no |
| 8 | $S_{NN4}$ | 180 | no | no |
| 9 | $S_{NN5}$ | 225 | no | no |
| 10 | $S_{NN6}$ | 270 | no | no |
| 11 | $S_{NN7}$ | 315 | no | no |
| 12 | $S_{YN1}$ | 45 | yes | no |
| 13 | $S_{YN2}$ | 90 | yes | no |
| 14 | $S_{YN3}$ | 135 | yes | no |
| 15 | $S_{YN4}$ | 180 | yes | no |
| 16 | $S_{YN5}$ | 225 | yes | no |
| 17 | $S_{YN6}$ | 270 | yes | no |
| 18 | $S_{YN7}$ | 315 | yes | no |
| 19 | $S_{NY1}$ | 45 | no | yes |
| 20 | $S_{NY2}$ | 90 | no | yes |
| 21 | $S_{NY3}$ | 135 | no | yes |
| 22 | $S_{NY4}$ | 180 | no | yes |
| 23 | $S_{NY5}$ | 225 | no | yes |
| 24 | $S_{NY6}$ | 270 | no | yes |
| 25 | $S_{NY7}$ | 315 | no | yes |
| 26 | $S_{YY1}$ | 45 | yes | yes |
| 27 | $S_{YY2}$ | 90 | yes | yes |
| 28 | $S_{YY3}$ | 135 | yes | yes |
| 29 | $S_{YY4}$ | 180 | yes | yes |
| 30 | $S_{YY5}$ | 225 | yes | yes |
| 31 | $S_{YY6}$ | 270 | yes | yes |
| 32 | $S_{YY7}$ | 315 | yes | yes |

computed from the NCPOM is used in NCWAM to compute the wave directional spectrum. The wave directional spectrum is used in the coupler to compute the new surface and bottom shear stresses, which are, in turn, used in the NCPOM model to compute the currents at the next time step.

## 4. Model Setting and Experiment Design

The model domain and bottom topography (Figure 2) used in this study are the same as those used by *Xie et al.* [1998]. The study area covers the coastal waters from the Georgia-South Carolina border in the South Atlantic Bight to the North Carolina-Virginia border in the Middle Atlantic Bight. The coastline, which is depicted as an infinite vertical wall at which the velocity component normal to the wall is zero, forms the western boundary of the model domain for both the circulation model and the wave model. The north, south, and east boundaries are open boundaries which are described, respectively, by the radiation boundary condition which allows gravity waves to propagate outward across the boundaries in the circulation model [*Mellor*, 1996] and by the no-gradient boundary condition in the wave model. The horizontal grid size is uniformly set to 5 km in both $x$ and $y$ directions. The $(x, y)$ coordinates are rotated 37° counter-clockwise from the latitude and longitude lines, respectively, to align the coast approximately with the $y$-axis. In the vertical direction, 18 σ levels are used.

The surface drag coefficient $C_D$ for all wave-current coupled runs is derived according to the coupling procedure described in section 3 and for stand-alone current model runs is based on the work of *Large and Pond* [1981]

$$C_D = \begin{cases} 1.14\times10^{-3} & U_0 \le 10 ms^{-1} \\ (0.49+0.065U_0)\times10^{-3} & U_0 > 10 ms^{-1} \end{cases} \quad (40)$$

In this study, we will focus on the effect of waves on circulation under constant wind conditions. First, four experiments (Cases NN, YN, NY, YY) under different wave-current coupling scenarios (Table 1) are designed to examine the relative contribution of wave-induced surface and bottom shear stresses to ocean currents. In these experiments a constant wind with a speed of 18.45 m $s^{-1}$ blowing from the northern to the southern boundary of the model domain is applied. The 18.45 $ms^{-1}$ wind speed has been chosen because it is the wind speed used in a number of other wave modeling studies [e.g., *Komen et al.*, 1994]. Then 28 experiments (Cases $S_{NN}$, $S_{YN}$, $S_{NY}$, and $S_{YY}$ in Table 1) with the same wind speed but different wind directions are conducted to examine the sensitivity of wave effects to wind directions. In all simulations the wave model and the current model are run for 24 hours.

In this study, we will focus on the effect of wave-induced surface and bottom shear stresses. To isolate these effects, we have switched off the wave-current coupling through the radiation stress.

## 5. Simulated Wind-Driven Circulation Under an Upwelling Favorable Wind

In this section the simulation results from the first four experiments listed in Table 1 (Cases NN, YN, NY, and YY) are presented. We will focus on the differences among the four cases and assess the relative importance of wave-induced surface and bottom shear stresses on the currents and sea surface elevation.

### 5.1. Simulated Wind-Driven Circulation in Case NN

Consider first the wind-driven circulation in the uncoupled case (Case NN). In this experiment the surface drag coefficient $C_D$ is computed from (40) [*Large and Pond*, 1981]. The bottom drag coefficient $C_b$ is set to a constant of 0.00375 as by *Davies and Lawrence* [1995]. The simulated near-surface and near-bed currents in Case NN are shown in Figures 3a and 3b. The contours in these figures represent the magnitude of the currents. The surface water level is shown in Figure 3c. The response of the coastal ocean is consistent with the "Ekman frictional equilibrium response" found in other parts of coastal waters [*Beardsley and Butman*, 1974; *Scott and Csanady*, 1976]. At the surface the near-shore currents are mainly parallel to the coastline, whereas the offshore surface currents are directed 30°-45° angle to the right (onshore) of the wind (Figure 3a). The magnitude of surface currents ranges from the order of 0.2–0.4 $ms^{-1}$ in deep water to about 1.2 m $s^{-1}$ in shallow water. Near the bottom the currents are also mainly parallel to the coastline near the coast but veer increasingly offshore as the water depth increases. The strongest bottom currents are of the order of 0.6 $ms^{-1}$ and occur near the coast. In response to the down-welling favorable south-southwestward wind, there is a 0.2-0.5 m coastal sea level setup accompanying the onshore surface flow (Figure

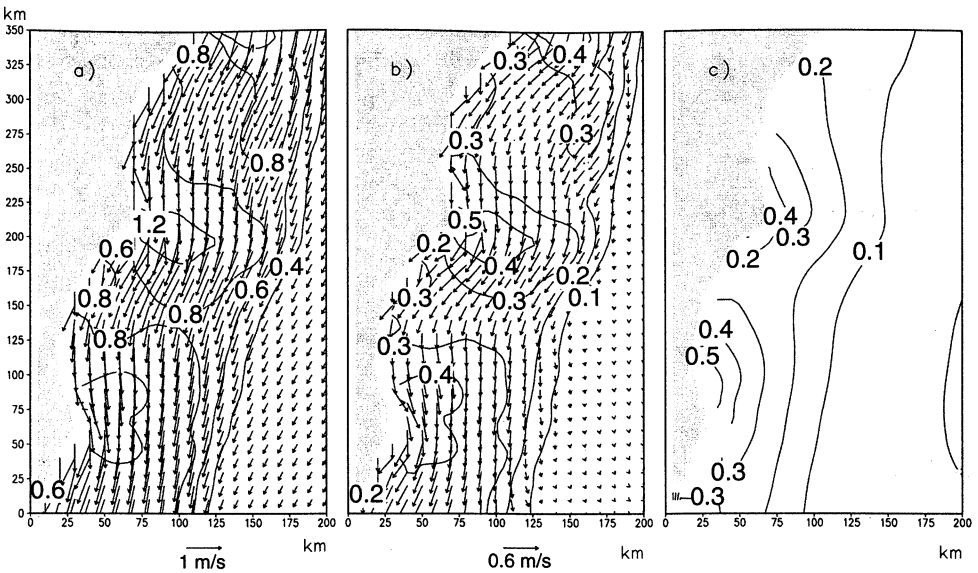


**Figure 3.** Simulated surface and bottom currents and sea level in Case **NN**: (a) surface current vectors, (b) as in (Figure 3a) but for bed currents, and (c) sea level anomalies. The contours in Figures 3a and 3b indicate current speed.

3c). The maximum setup occurs along the southern portion of the Capes.

### 5.2. Simulated Wind-Driven Circulation in Case YN

In Case YN the coupling between currents and waves is only through wave-induced surface shear stress. This is done through (21) [*Donelan et al.*, 1993], which shows that the surface drag coefficient depends on both wind speed and wave state. The latter is characterized by the spectral peak frequency of the wave frequency spectrum. The predicted spectral peak frequency from the wave model combined with the magnitude of wind speed at each grid point determines the value of the drag coefficient at that

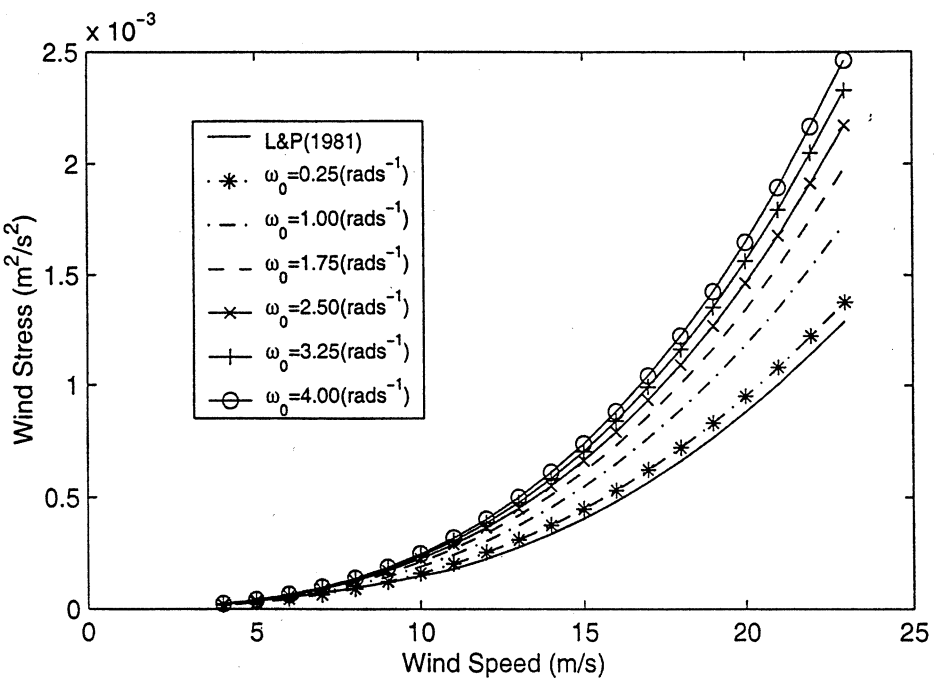


**Figure 4.** Wind stresses computed using different drag coefficients. The smooth solid curve shows the wind stress as a function of wind speed based on the drag coefficient of *Large and Pond* [1981]. The rest six curves represent the wind stresses based on the wave-modified drag coefficient proposed by *Donelan et al.* [1993] under different peak wave frequency.

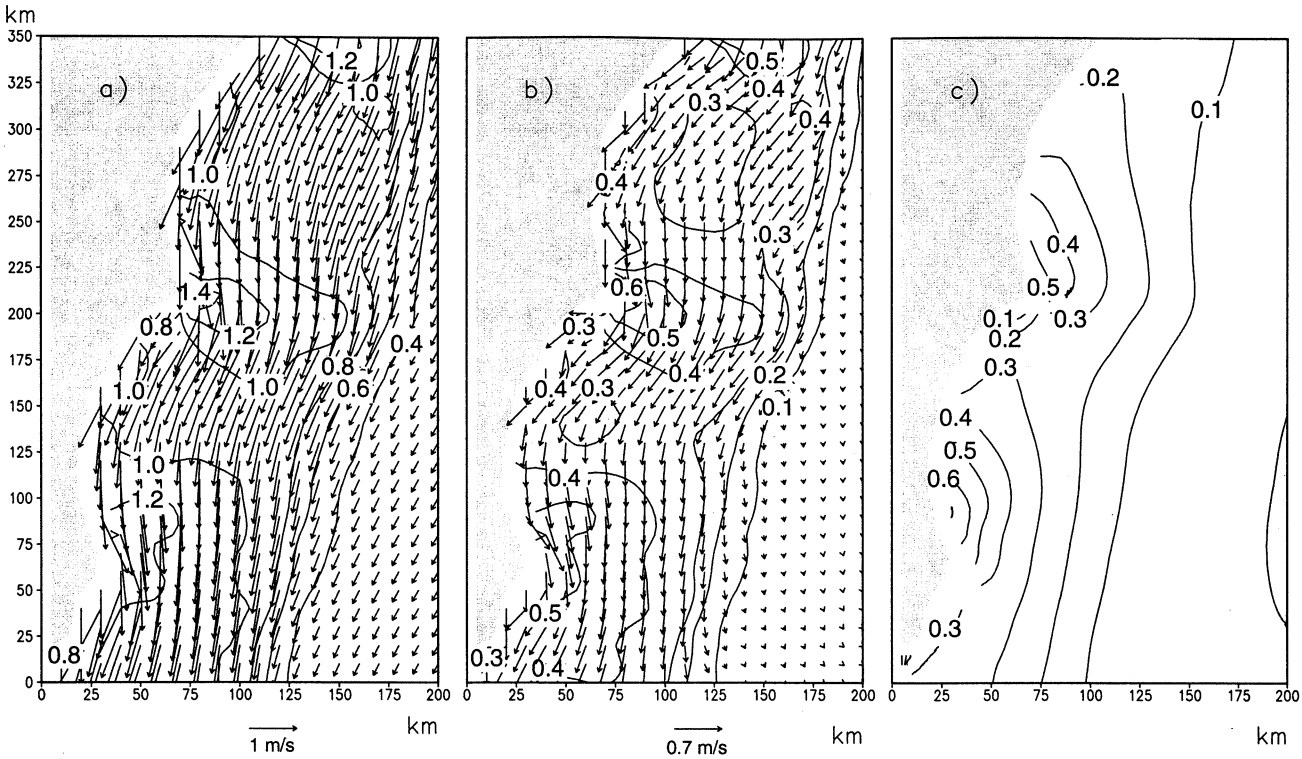


**Figure 5.** Same as Figure 3, but for Case YN.

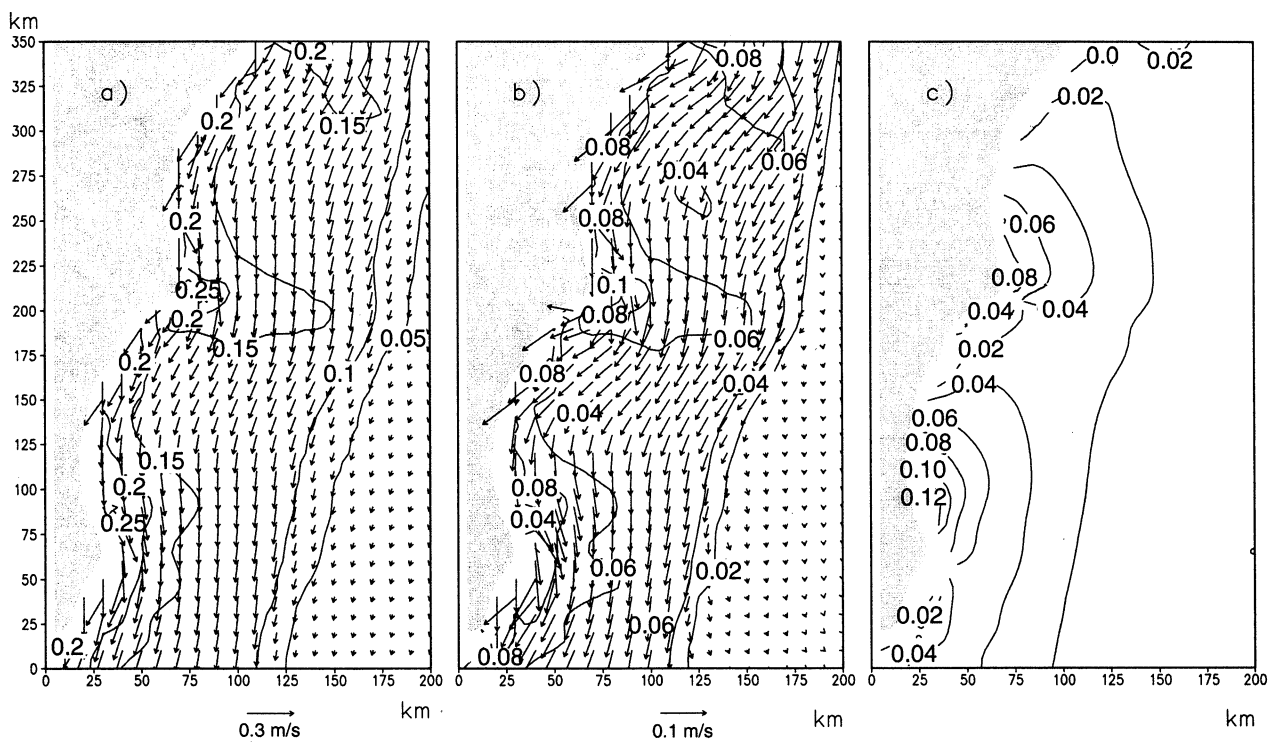


**Figure 6.** The difference between Cases YN and NN. (a) The difference vector between the surface currents in Case YN and those in Case NN (i.e., Case YN-Case NN), (b) same as (Figure 6a, but for bottom currents, (c) The difference of sea level (in meters) between Cases YN and NN (i.e., Case YN-Case NN). The contours in Figures 6a and 6b indicate the magnitude of vectors (in m $s^{-1}$).

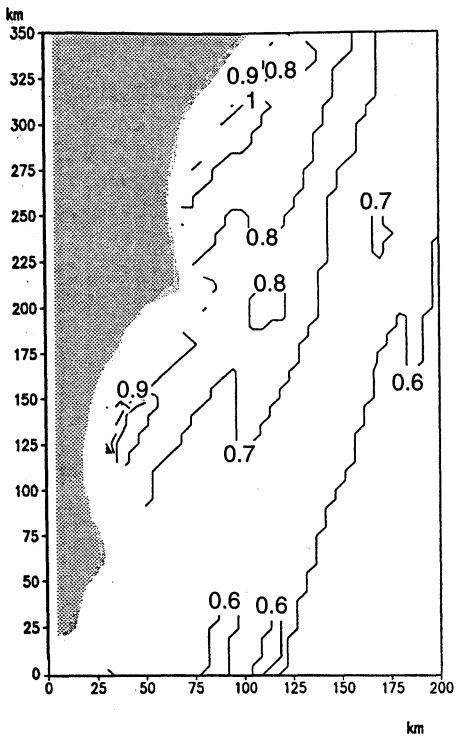


**Figure 7.** Spectral peak frequencies. It indicates that higher spectral peak frequencies occur in shallow waters near the coast, while relatively lower spectral peak frequencies occur in deep waters.

location. Once the drag coefficient is determined, the surface shear stress can be computed from the quadratic stress law (4). The modulation of surface shear stress by waves is illustrated in Figure 4. The surface shear stresses based on *Donelan et al.* [1993] (dashed curves) under different wind speed and sea state conditions are generally larger than that based on the surface drag coefficient of *Large and Pond* [1981] (solid curves). The modification of the surface shear stress by surface waves increases significantly as the wind speed or wave frequency increase. For example, at a wind speed of 18.45 m $s^{-1}$ and a spectral peak frequency of 4 rad $s^{-1}$, the magnitude of the surface shear stress based on the drag coefficient of *Donelan et al.* [1993] is approximately 80% larger than that based on the drag coefficient of *Large and Pond* [1981]. Comparisons between the solid and the broken curves in Figure 4 indicate that the modification of surface shear stress is closely related to wave age changes. For young waves the spectral peak frequency is large, and accordingly, the wave-induced surface stress is large. However, for fully developed wind waves the spectral peak frequency is small and accordingly the effect of waves on surface stress is relatively small.

The wave-enhanced surface shear stress in Case YN resulted in significant increases in surface and bottom currents (Figures 5a and 5b), as well as coastal sea level setup (Figure 5c). The maximum surface current speed exceeded 1.4 m $s^{-1}$ and the maximum bottom current speed exceeded 0.6 m $s^{-1}$ near Cape Fear, North Carolina. The highest coastal sea level setup increased to 0.7 m off the coast of South Carolina.

The effect of waves on currents can be further illustrated in the difference fields of currents and sea level between Cases YN and NN (Figures 6a-6c). Both surface and bottom currents are generally stronger in Case YN than in Case NN as indicated by the southward vector current differences. The largest difference in the surface current field reached 0.3 m $s^{-1}$ or about 25% of the value in Case NN. The largest difference in the bottom current field is about 0.1 m $s^{-1}$, or 15% of its value in Case NN. The strongest modifications of currents near the surface and at the bottom are both near the coast and shoals in the shallow waters. As the water depth increases, the effect of waves decreases rapidly. Figure 6c is a plot of the water level difference between Cases YN and NN. A significant increase of water level in Case YN (0.1-0.13 m or 15-25% of its value in Case NN) can be found near the coast. Similar to currents, as the water depth increases, the difference of water level between Cases YN and NN decreases. Thus the effect of wind waves appears to be more pronounced in coastal waters. This is because under a constant wind the magnitude of the wind stress increases as the wave spectral peak frequency increases (Figure 4). As shown in Figure 7, the wave spectral peak frequency $\omega_0 (=2\pi f)$ increases as the water depth decreases. The magnitude of the wave peak spectral frequency $\omega_0$ increases from about 0.6 rad $s^{-1}$ in the relatively deep offshore water to approximately 0.9-1.0 rad $s^{-1}$ in the shallower coastal water. As a consequence, under a constant wind the effect of waves on wind stress is larger in the shallower water than in the deeper water.

### 5.3. Simulated Wind-Driven Circulation in Case NY

In this subsection, we will primarily examine how the wind-driven circulation and sea level are modified by wave-induced bottom stress. This is done by comparing the results in Case NY, where the currents and waves are coupled only through wave-induced bottom stress, and those in Case NN. The effect of wave-induced bottom stress on currents has been studied by *Davies and Lawrence* [1995], where the effect of waves on bottom stress is simulated by using a three-dimensional circulation model with a prescribed wave field, which has a constant amplitude and period. Here we will take a somewhat similar approach, and the coefficients associated with the bed drag coefficient $f_c$, such as $z_r$ and $z_0$, are set to the same values as those used by *Davies and Lawrence* [1995]. However, in this study we will prescribe the wind field, not the wave field. The latter will be simulated using the wave model under realistic coastal topographic setting. Thus the wave field used here will have variable amplitude and period and is thus more realistic.

Figures 8a and 8b show the simulated surface and bottom currents. The wind is again blowing toward the southern boundary of the model domain as in Cases NN and YN. The general circulation pattern is similar to that in Case NN (Figures 3a and 3b). However, differences in magnitude are evident in shallow water regions. The currents are generally weaker, especially near the bottom. The maximum surface current is reduced about 0.4 m $s^{-1}$ from 1.2 to 1.3 m $s^{-1}$ in Case NN to 0.8-0.9 m $s^{-1}$ in case NY. This represents a weakening of 25-35%. The largest bottom current is weakened by over 50% in shallow waters (from more than 0.6 m $s^{-1}$ in case NN to less than 0.3 m $s^{-1}$ in Case NY). These large changes in current speed in shallow waters near the coast indicate the strong influences of wave-induced bottom stress. Figure 8c depicts the water level in Case NY. Clearly, the reduction in current speed resulted in a smaller coastal sea level setup. The maximum setup decreased from 0.5-

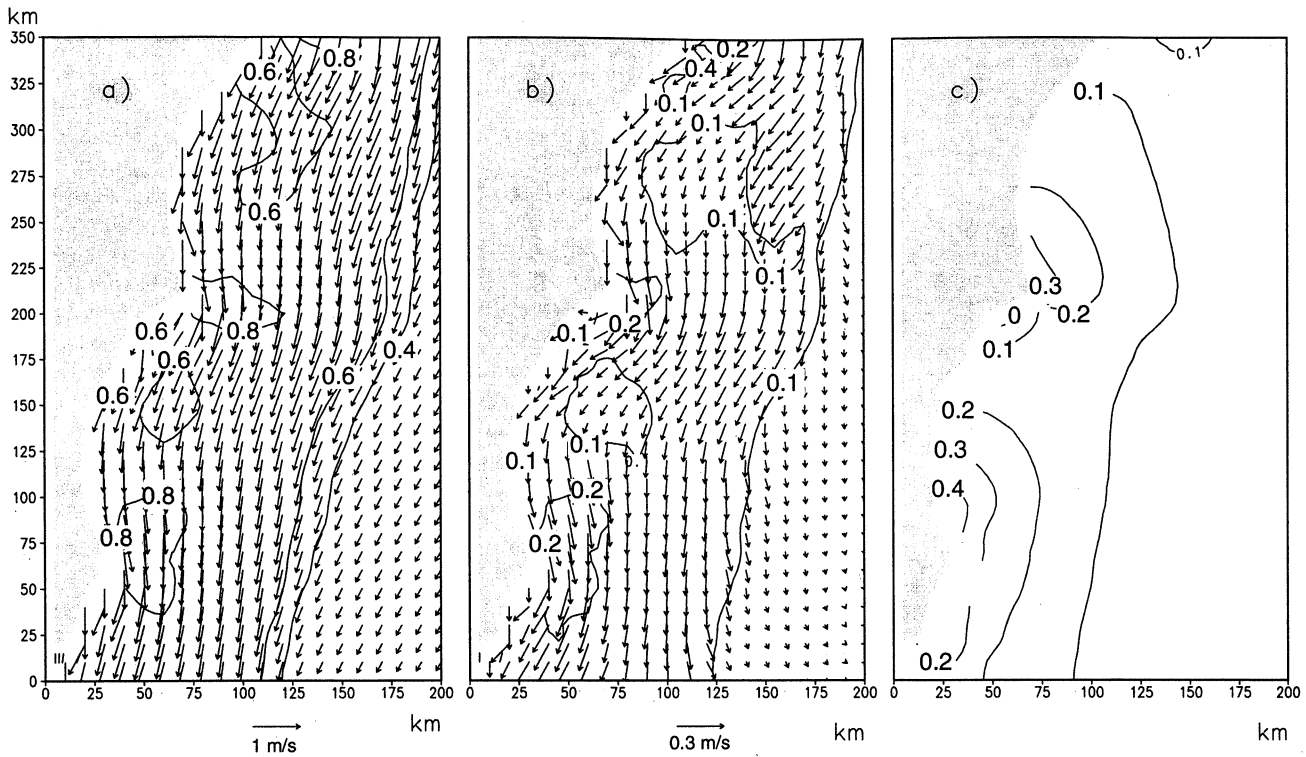


**Figure 8.** Same as Figure 3, but for Case NY.

0.6 m in Case NN to 0.4-0.5 m in Case NY, a reduction of 10-20%.

To understand the effect of waves on bottom stress, we will examine the distribution of wave period (Figure 9a). It shows that the wave periods range from 2 to 3 s in very shallow waters to 9 to 10 s in deep waters. On the continental shelf the typical wave period is 7-8 s. The distributions of significant wave heights as well as the wave directions are shown in Figure 9b. The wave height varies from 1 m near the coastline to 6 m in the deep water. From the wave direction distributions (the vector field) the phenomenon of wave refraction induced by bottom topography and wave-current interaction is clearly shown (influence of currents on waves will be discussed elsewhere). From Figures 9a and 9b it is seen that even under constant meteorological conditions the wave fields cannot be considered uniform. Thus in the computation of bottom friction, spatially non-uniform wave fields should be used.

Compared with Cases NN and YN discussed earlier, the effect of waves on the bottom stress was found to dampen both surface and bottom currents as well as reduce water level near the coast. However, in Case YN, wave effects on the surface stress were found to cause an increase of surface and bed currents and sea level. Thus surface waves produce two opposite effects on the circulation: energy input through surface stress and energy dissipation through bottom stress. Thus it is important to quantify these two effects and understand the net effect of waves.

To quantify the effect of wind-induced bottom stress, the differences of wind-induced surface and bottom currents between Cases NN and NY are plotted (Figures 10a and 10b). Note that for the convenience of comparing with Figures 6a and 6b, the difference in Figures 10a and 10b is chosen in the opposite sense (i.e., Case NN-Case NY) as that in Figures 6a and 6b, so the prevailing direction of the vectors remains the same (southward) as that in Figures 6a and 6b. It is shown that the maximum decrease in both surface and bottom currents due to wave-induced bottom stress is more than 0.30 m $s^{-1}$ (Figures 10a and 10b) near the coast. The decreases of currents, both at the sea surface and at the seabed, are of the order of 0.10 m $s^{-1}$ in offshore waters. The sea level difference between the two cases is also plotted (Figure 10c). Again the difference is in the opposite sense of that in Figure 6c, that is, Case NY-Case NN. The water levels were found to decrease from the order of 0.00-0.05 m in the relatively deep water to the order of 0.10-0.15 m near the coast (Figures 10c).

### 5.4. Simulated Circulation in Case YY

The effect of surface waves on the surface and bottom stresses were examined separately in sections 5.2 and 5.3. Generally, surface waves affect both surface and bottom stresses. In order to examine the net effect of surface waves on ocean currents, both the wave-induced surface and bottom stress effects must be studied together. This is considered in Case YY.

The simulated current fields in Case YY are shown in Figures 11a and 11b. The general flow patterns are similar to those found in Cases NN (Figures 3a and 3b), YN (Figures 5a and 5b) and NY (Figures 8a and 8b), but there are quantitative differences. To quantify the differences between Cases YY and NN, we plotted the differences of surface and bottom currents between Cases NN and YY in Figures 12a and 12b. The difference in Figures 12a and 12b is in the same sense as that in Figures 6a and 6b, that is, currents in Case NN are subtracted from those in Case

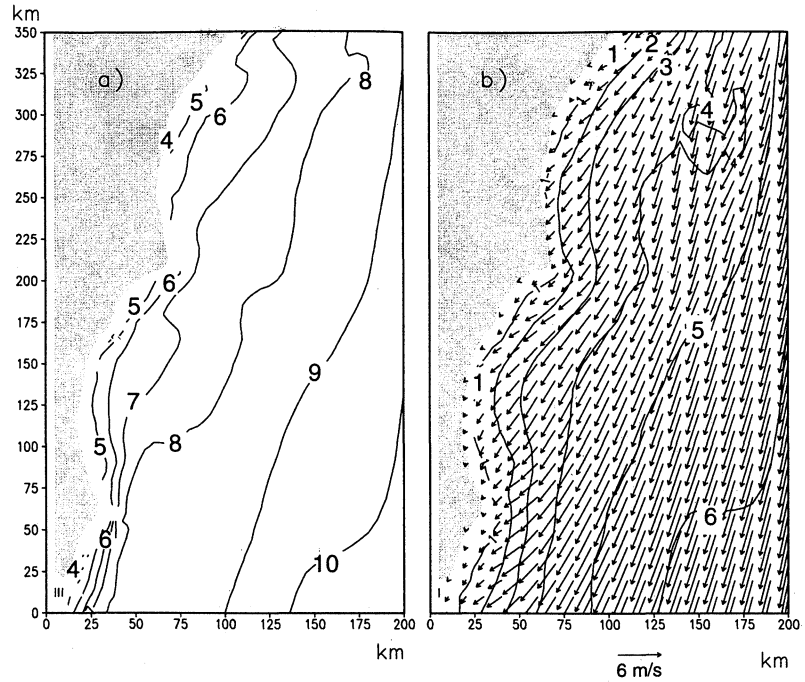


**Figure 9.** Mean wave period and significant wave height in Case NY. (a) Mean wave period (second); and (b) significant wave height (meter).

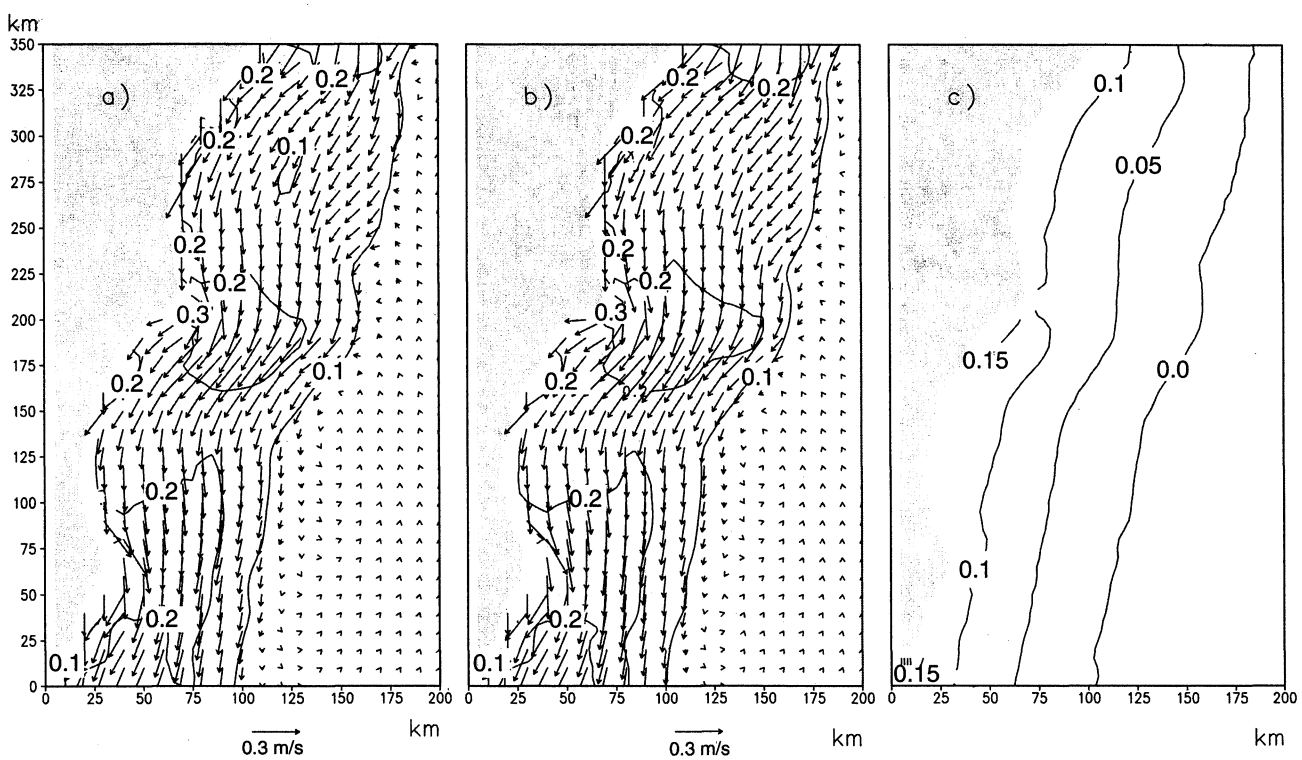


**Figure 10.** Same as Figure 6, but for the difference between Cases NN and NY. Note that for the convenience of comparing with Figure 6, the difference in this figure is in the opposite sense (i.e., Case NN-Case NY) as that in Figure 6, so the prevailing direction of the vectors in Figures 10a and 10b remains the same (southward) as that in Figures 6a and 6b.

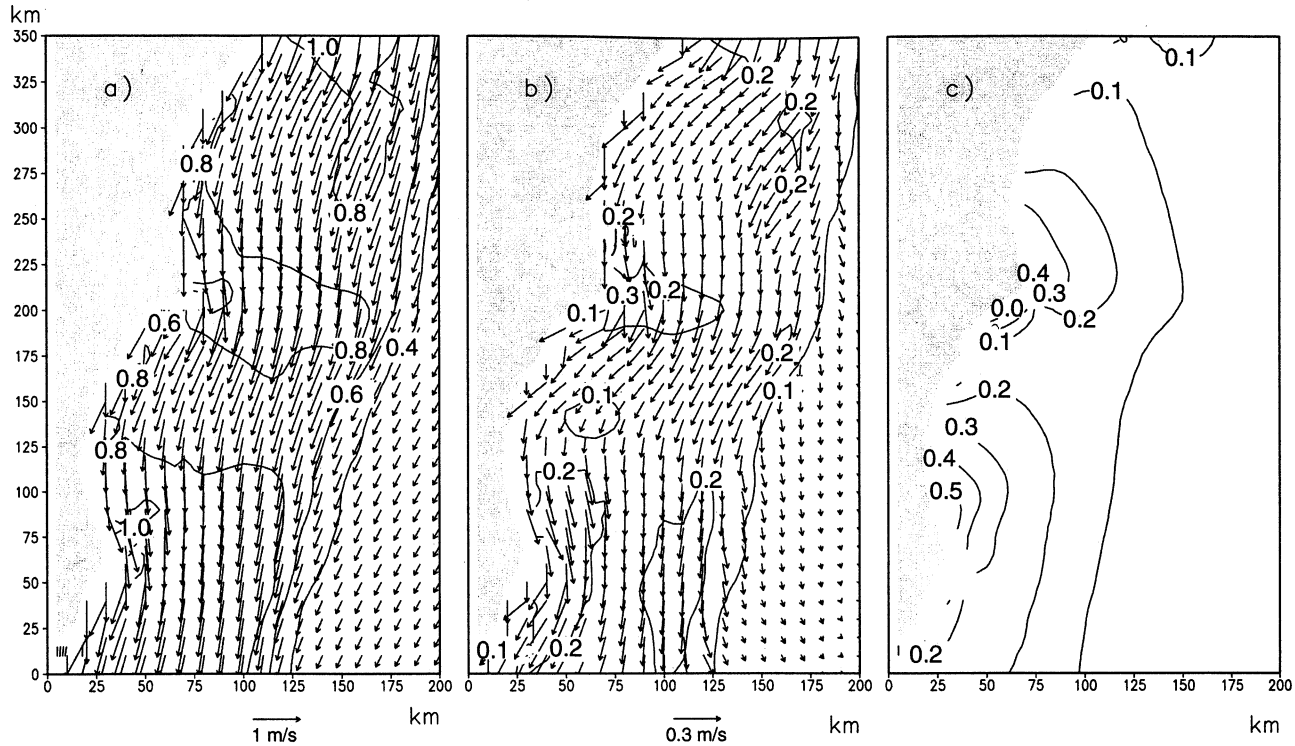


**Figure 11.** Same as Figure 3, but for Case YY.

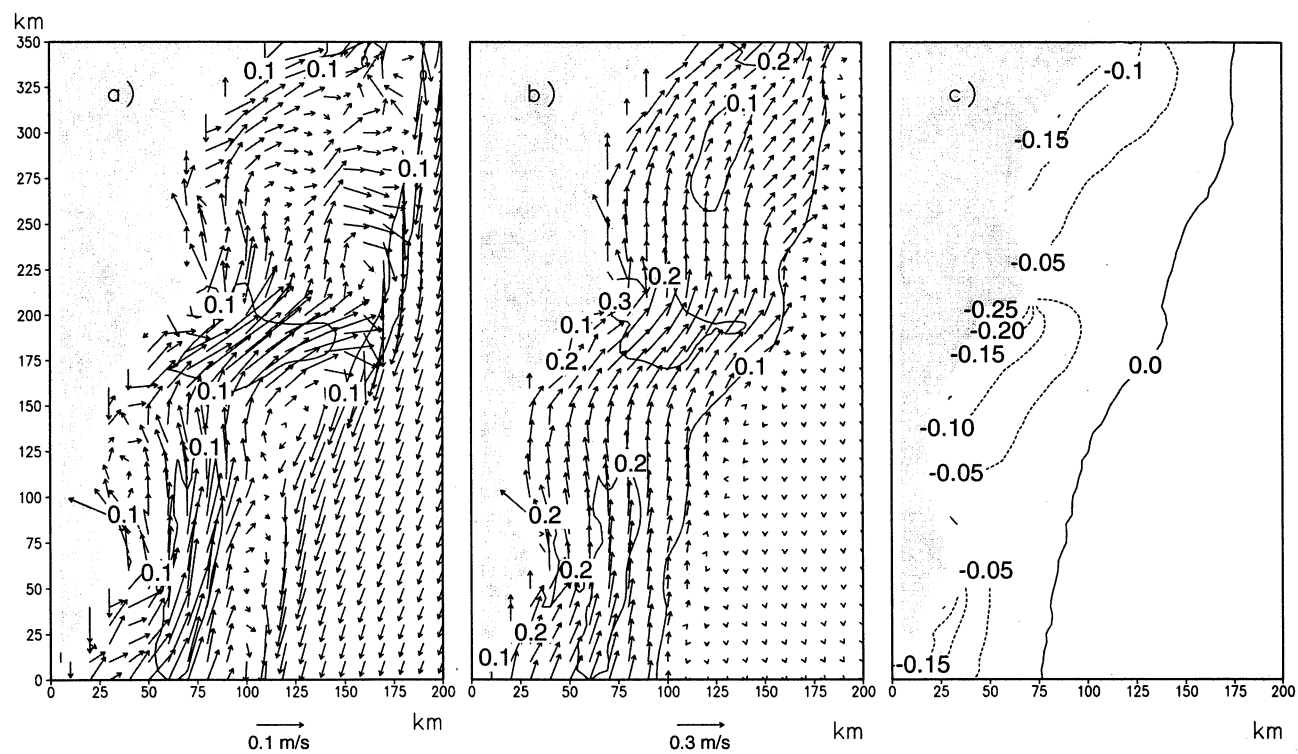


**Figure 12.** Same as Figure 6, but for the difference between Cases YY and NN. Note that the difference in this figure is in the same sense as that in Figure 6 (i.e., Case YY-Case NN), so the prevailing direction of the vectors in Figures 12a and 12b remains the same (southward) as that in Figures 6a and 6b.

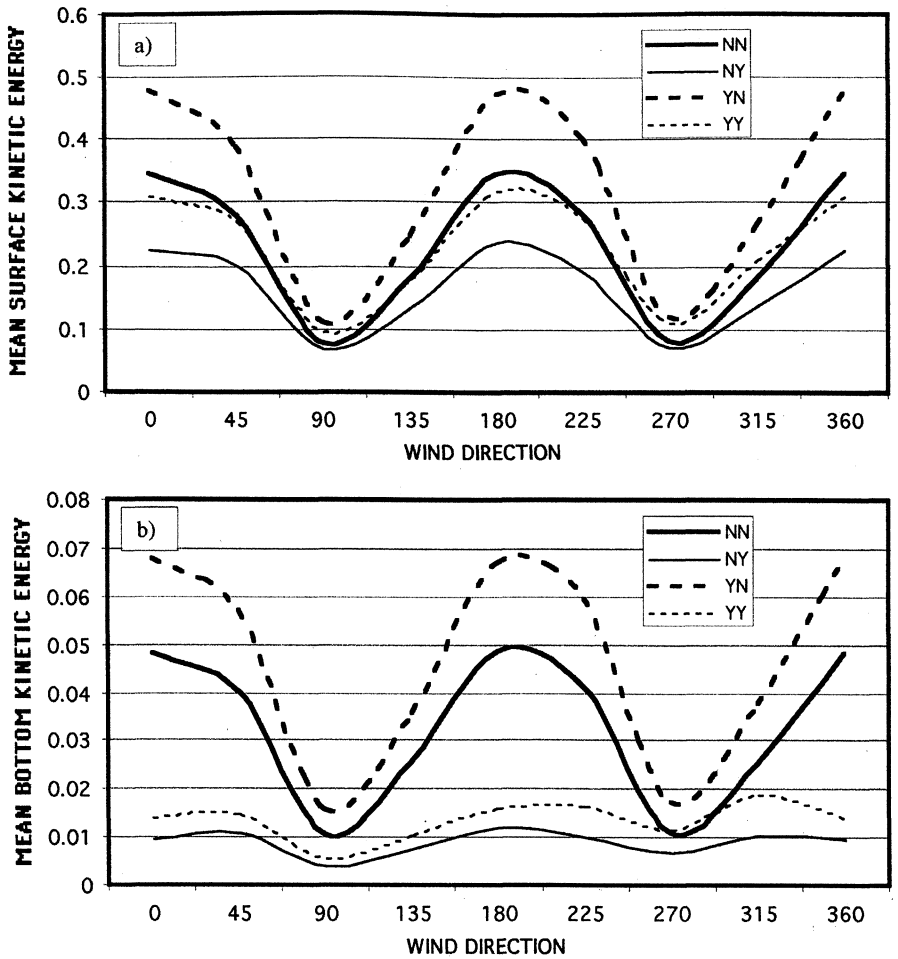


**Figure 13.** Mean kinetic energy averaged over the model output domain as a function of wind direction for the sensitivity cases. (a) Mean surface kinetic energy and (b) mean bottom kinetic energy. NN is for cases without wave effects (Cases $S_{NN}$), YN is for cases without wave-induced bottom stress effect (Cases $S_{YN}$), NY is for cases without wave-induced surface stress effect (Cases $S_{NY}$), and YY is for cases considering both wave-induced surface and bottom stresses (Cases $S_{YY}$).

YY. The difference vectors near the coast are predominantly opposite to those offshore. Near the coast the vectors are mainly southward (in the same direction as the actual current), indicating a weakening by the net wave effects. In the offshore waters the vectors are generally northward (but smaller than those near the coast), indicating an enhancement by the net wave effect. The maximum decrease in the magnitude of surface currents due to the inclusion of wave effects on both wind stress and bottom stress is 0.1-0.2 m $s^{-1}$ (15%). However, in offshore waters the surface currents are about 0.1 m $s^{-1}$ stronger in Case YY than in Case NN (Figure 12a). The bed currents in Case YY are generally weaker than in case NN when wave effects are considered in both wind stress and bottom stress. The maximum bottom current in Case YY is about 0.3 m $s^{-1}$ weaker than in Case NN. Figure 12c shows the differences of water level between Cases NN and YY (Case YY-Case NN). The water level differences are from 0.2 to 0.25 m with a lower value in Case YY. However, the largest differences are located along the northern portions of the Carolina Capes, which is out of phase with the high water level along the southern portion of the Capes (Figure 11c).

## 6. Sensitivity to Wind Direction

The southwestward alongshore wind cases discussed in section 5 indicated that the damping effect of wave-induced bottom stress can be more significant than the enhancement effect of wave-induced wind stress in some areas of the shallow coastal waters. However, as we will show below, the combined (net) effect of wave-induced wind and bottom stresses can be quite different under different wind directions. Here we will examine the sensitivity of the net effect of wave-induced surface and bottom shear stresses on coastal currents and sea level to wind direction changes. The wind speed is kept the same as that used earlier (18.45 m $s^{-1}$), but the directions vary from 0° (or 360°) ($u$ = 0, $v$= -18.45 m $s^{-1}$), to 315° ($u$ = 13.05 m $s^{-1}$, $v$ = -13.05 m $s^{-1}$) at an interval of 45° (Table 1).

In order to quantify the effect of surface waves on the coastal circulation under different wind directions, the domain-averaged kinetic energy at the sea surface and that near the bottom are computed for each wind direction (Cases $S_{NNi}$, $S_{YNi}$, $S_{NYi}$, and $S_{Yyi}$, where I=1,2,3,...,7). The results are shown in Figure 13a (for surface kinetic energy) and Figure 13b (for bottom kinetic

energy). The various curves depict the mean kinetic energy change as a function of wind direction in Cases $S_{NN}$ (thick solid curve), $S_{YN}$ (thick dash curve), $S_{NY}$ (thin solid curve), and $S_{YY}$ thin dash curve). The largest kinetic energy in both surface and bottom current fields was found in Cases $S_{YN}$. Thus wave-current interaction through surface stress alone enhances the currents throughout the water column. In other words, wind waves increase the input of wind energy into the ocean. On the other hand, the smallest kinetic energy in both surface and bottom current fields occurred in Cases $S_{NY}$. This suggests that wave-current interaction through bottom stress alone always decreases the kinetic energy throughout the water column. In other words, wave-induced bottom stress acts as a dissipation mechanism not only for bottom currents but also for currents throughout the entire water column. The mean surface kinetic energy in Cases $S_{YY}$ is somewhat larger (smaller) than that in Cases $S_{NN}$ for winds with directions roughly from 50° to 130° and from 230° to 325° (0° to 50° and 130° to 180°). Thus for winds blowing predominantly alongshore (cross-shore), wave-induced bottom shear stress is more (less) important than the wave-induced surface shear stress. In other words, the net wave-induced surface and bottom shear stress effect can either enhance or damp the surface current, depending on the wind direction. For the kinetic energy in the near-bed flow, the effect of wave-induced bottom shear stress is larger than that of the wave-induced surface shear stress for all wind directions. As a result, the mean kinetic energy of the near-bed flow in Cases $S_{NN}$ is generally larger than that in Cases $S_{YY}$ except for direct offshore winds (Figure 13b). The difference of mean near-bed kinetic energy between Cases $S_{YY}$ and $S_{NN}$ is larger for alongshore than for cross-shore winds. In fact, there is almost no difference for direct offshore winds (wind direction ~ 270°). Thus surface waves generally cause a damping effect on the near-bed flow and this damping effect increases as the winds rotate either clockwise or counterclockwise from cross-shore directions toward alongshore directions.

## 7. Conclusions

Previous studies have shown that surface waves can increase ocean currents by enhancing the wind stress [e.g., *Donelan et al.*, 1993] and decrease the ocean currents by enhancing the bed stress [e.g., *Davies and Lawrence*, 1995]. The former effect generally leads to an increase in coastal storm surge (or sea level change) [*Komen et al.*, 1994]. Our study suggests that in order to estimate the net effect of wind waves on ocean currents and sea level change, the effects of wave-induced surface and bottom shear stresses must be examined simultaneously. Although wind waves generally increase the magnitude of currents, both at the sea surface and at the seabed, through wave-induced surface shear stress, wave-induced bottom shear stress can play a significant and even dominant balancing role in wave-current interaction. The relative importance of wave-induced surface and bottom shear stresses in wave-current interaction depends on the surface wind field. For the constant wind speed (18.45 m $s^{-1}$) considered in this study, it is shown that the effect of wave-induced bottom stress is more significant for along-shore winds than for cross-shore winds. The results of this study also indicate that the effect of waves on currents is mainly present in shallow coastal waters and attenuates rapidly offshore as water depth increases. This is consistent with the results found in other studies [e.g., *Davies and Lawrence*, 1995].

It should be noted that the results presented above are derived from a specific wind speed (18.45 m $s^{-1}$). As we will show in part 2 of this study, the effects of wave-induced surface and bottom shear stresses also depend on the wind speed. In tropical cyclone situations the effect of wave-induced surface shear stress is generally more important than that due to wave-induced bottom shear stress, and hence the effect of wind waves usually increases the magnitude of storm surge. It should also be noted that in order to fully understand the effect of waves on coastal ocean circulation, the turbulence closure scheme used in the POM model to determine the diffusion coefficient must consider the effect of waves on the energy flux across the air-sea interface. The present study focuses on the combined effects of wave-induced surface and bottom stresses on coastal ocean circulation, and it is beyond the scope of the present study to address the dynamical coupling between surface waves and turbulence closure.

**Acknowledgments.** We thank Norden E. Huang and Yeli Yuan for helpful suggestions and comments. An anonymous reviewer provided constructive comments which helped to improve the final version of the manuscript. This study is supported by the Office of Naval Research (ONR) through grant N00014-98-1-0652 and National Oceanic and Atmospheric Administration through grant NA06OC0373.

## References

Beardsley, R.C., and B. Butman, Circulation on the New England continental shelf: Response to strong winter storms, *Geophys. Res. Lett. 1*, 181-184, 1974.

Christofferson, J.B., and I.G. Jonsson, Bed friction and dissipation in a combined current and wave motion, *Ocean Eng., 12*, 387-423, 1985.

Davies, A.M., and J. Lawrence, Modeling the effect of wave-current interaction on the three-dimensional wind-driven circulation of the eastern Irish Sea, *J. Phys. Oceanogr., 25*, 29-45, 1995.

Donelan, W.A., F.W. Dobson, and S.D. Smith, On the dependence of sea surface roughness on wave development, *J. Phys. Oceanogr., 23*, 2143-2149, 1993.

Grant, W.D., and O.S. Madsen, Combined wave and current interaction with a rough bottom, *J. Geophys. Res., 84*, 1797-1808, 1979.

Hasselmann, S., and K. Hasselmann, Computations and parameterizations of the nonlinear energy transfer in a gravity wave spectrum, I; A new method for efficient computations of the exact nonlinear transfer integral, *J. Phys. Oceanogr., 15*, 1369-1377, 1985.

Hasselmann, K., et al., Measurements of wind-wave growth and swell decay during the Joint North Sea Wave Project (JONSWAP), *Dtsch. Hydrogr. Z. Suppl. A, 8*(12), 95 pp., 1973.

Hasselmann, S., Hasleman, K., Allender, J.H., and T.P. Barnett, Computations and parameterizations of the nonlinear energy transfer in a gravity wave spectrum, II, Parameterizations of the nonlinear energy transport for application in wave models, *J. Phys. Oceanogr., 15*, 1378-1391, 1985.

Holthuijsen, L.H. and H.L. Tolman, Effects of the Gulf Stream on ocean waves, *J. Geophys. Res., 96*, 12,755-12,771, 1991.

Huang, N.E., On surface drift currents in the ocean, *J. Fluid Mech., 91*, 191-208, 1977.

Jenkins, A.D., Wind and wave induced currents in a rotating sea with depth-varying eddy viscosity, *J. Phys. Oceanogr.*, 17, 938-951, 1987.

Jonsson, I.G., Wave boundary layers and friction factors, in *Proceedings of 10th International Conference on Coastal*

*Engineering 1966*, pp. 127-148, Am. Soc. of Civ. Eng, Reston, VA., 1967.

Jonsson, I.G., and N.A. Carlsen, Experimental and theoretical investigations in an oscillatory turbulent boundary layer, *J. Hydraul. Res., 14*, 45-60, 1976.

Komen, G.,K. Hasselmann, and S. Hasselmann, On the existence of a fully developed wind sea spectrum, *J. Phys. Oceanogr., 14*, 1271-1285, 1984.

Komen, G.J., Cavaleri, L., Donelan, M., Hassleman, K., Hassleman, S., and P.A.E.M., Janssen, *Dynamics and Modeling of Ocean Waves*, 532 pp., Cambridge Univ. Press, New York, 1994.

Large, W.G., and G.B. Crawford, Observations and simulations of upper-ocean response to wind events during the ocean storm experiment, *J. Phys. Oceanogr., 25*, 2831-2852, 1995.

Large, W.G., and S. Pond, Open ocean momentum fluxes in moderate to strong winds, *J. Phys. Oceanogr., 11*, 324-336, 1981.

Lewis, J.K., A three-dimensional ocean circulation model with wave effects: Estuarine and coastal modeling, in *Proceedings of the Fifth International Conference*, edited by M.L. Spaulding and A.F. Blumberg, Am. Soc. of Civ. Eng., Reston, VA, 1998.

Lin, Ray Q., Norden E. Huang, The Goddard coastal wave model. Part I: Numerical method. *J. Phys. Oceanogr.* 26, 833–847, 1996a.

Lin, Ray Q., Norden E. Huang, The Goddard coastal wave model. Part II: Kinematics. *J. Phys. Oceanogr.* 26, 848–862, 1996b.

Longuet-Higgins, M.S., and R.W. Stewart, Radiation stress and mass transport in gravity waves, with application to "surf-beats," *J. Fluid Mech., 10*, 529-549, 1962.

Masson, D., A case study of wave-current interaction in a strong tidal current, *J. Phys. Oceanogr., 26*, 359-372, 1996.

Mastenbroek, C., G. Burgers, and P.A.E.M. Janssen, The dynamical coupling of a wave model and a storm surge model through the atmospheric boundary layer, *J. Phys. Oceanogr., 23*, 1856-1866, 1993.

Mellor, G.L., *Users Guide for a Three Dimensional, Primitive Equation Numerical Ocean Mode*, 39 pp., Princeton Univ. Press, Princeton, N.J., 1996.

Mellor, G.L., and T. Yamada, Development of a turbulent closure model for geophysical fluid problems, *Rev. Geophys., 20*, 851-875, 1982.

Miles, J., On the generation of surface waves by shear flows, *J. Fluid Mech., 3*, 185-204, 1957.

Phillips, O.M., The *Dynamics of Upper Ocean*, 336 pp., Cambridge Univ. Press, New York, 1977.

Scott, J.T., and G.T. Csanady, Nearshore currents off Long Island, *J. Geophys. Res., 81*, 5401-5409, 1976.

Signell, R.P., R.C. Beardsley, H.C. Graber, and A. Capotondi, Effect of wave-current interaction on wind-driven circulation in narrow, shallow embayments, *J. Geophys. Res., 95*, 9671-9678, 1990.

Smagorinski, J., Generic circulation experiments with primitive equations, I. The basic experiment, *Mon. Wea. Rev., 91*, 99-164, 1963.

Smith, S.D., et al., Sea surface wind stress and drag coefficients: The Hexos results, *Boundary Layer Meteorol., 60*, 109-142, 1992.

Snyder, R.L., F.W. Dobson, J.A. Elliott, and R.B. Long, Array measurements of atmospheric pressure fluctuations above surface gravity waves, *J. Fluid Mech., 102*, 1-59, 1981.

Tolman, H.L., The influence of unsteady depths and currents of tides on wind wave propagation in shelf seas, *J. Phys. Oceanogr., 20*, 1166-1174, 1990.

Tolman, H.L., A third generation model for wind waves on slowly varying, unsteady, and inhomogeneous depths and currents, *J. Phys. Oceanogr., 21*, 782-797, 1991.

Xie, L., L.J. Pietrafesa, and S. Raman, Coastal ocean-atmosphere coupling, in *Coastal Ocean Prediction, Coastal Estuarine Stud.,* vol. 56, edited by C.N.K. Mooers, pp. 101-123, AGU, Washington, D.C. 1999a.

Xie, L., L.J. Pietrafesa, and C. Zhang, Subinertial response of the Gulf Stream System to Hurricane Fran of 1996, *Geophys. Res. Lett., 26*. 3457-3460, 1999b.

Xie, L.A., L.J. Pietrafesa, E. Bohm, C. Zhang, and X. Li, Evidence and mechanism of Hurricane Fran-induced ocean cooling in the Charleston trough, *Geophys. Res. Lett., 25*, 769-772, 1998.

Xue, H.J. and J.M. Bane Jr., A numerical investigation of the Gulf Stream and its meanders in response to cold air outbreaks, *J. Phys. Oceanogr., 27*, 2606-2629, 1997.

---

L. J. Pietrafesa, L. Xie, and C. Zhang, Department of Marine, Earth and Atmospheric Sciences, North Carolina State University, Box 8208, Raleigh, NC 27695-8208. (lian_xie@ncsu.edu; len_pietrafesa@ncsu.edu).

K. Wu, Institute of Physical Oceanography, Ocean University of Qingdao, Qingdao, P. R. China.

(Received February 24, 2000; revised December 11, 2000; accepted April 17, 2001.)